

Article

Linear Voltage Stability Indicator (LVSI) for Optimal Placement of SVC Devices to Improve the Voltage Stability Margin in Transmission Systems

Christian Garrido , Alexander Aguila Téllez *  and Leony Ortiz 

Electrical Engineering Career, Universidad Politécnica Salesiana, Quito 170606, Ecuador

* Correspondence: aaguila@ups.edu.ec

Abstract: This study presents a procedure for placing static var compensators (SVC) in an EPS using the fuzzy *c*-means clustering technique. For this purpose, the optimal power flow (OPF) is initially quantified to obtain the sensitivity array of the system based on the Jacobian of the system. Then, the attenuation and electrical distance matrices are estimated. Subsequently, the fuzzy *c*-means clustering algorithm is used with the initially estimated cluster identification criterion to obtain the voltage control areas (VCAs). On the other hand, the criterion of minimizing the installation costs of the SVCs is used in conjunction with the linear voltage stability index (LVSI) for the ideal arrangement of the compensators. This is applied to each VCA created. The technique described is applied to the 14-node and 30-node schemes to check their effectiveness. Additionally, the results obtained are compared with the Power Factory software and with similar studies. Finally, the proposed technique proves to be effective for the creation of VCAs and for the optimal placement of SVC equipment.

Keywords: voltage control areas; fuzzy *c*-means clustering algorithm; SVC; linear voltage stability indicator; FACTS; voltage profile



Citation: Garrido, C.; Aguila Téllez, A.; Ortiz, L. Linear Voltage Stability Indicator (LVSI) for Optimal Placement of SVC Devices to Improve the Voltage Stability Margin in Transmission Systems. *Electronics* **2023**, *12*, 43. <https://doi.org/10.3390/electronics12010043>

Academic Editors: Majid Astaneh, Andrew McGordon and Vitor Monteiro

Received: 11 November 2022

Revised: 9 December 2022

Accepted: 19 December 2022

Published: 22 December 2022



Copyright: © 2022 by the authors. Licensee MDPI, Basel, Switzerland. This article is an open access article distributed under the terms and conditions of the Creative Commons Attribution (CC BY) license (<https://creativecommons.org/licenses/by/4.0/>).

1. Introduction

Reactive power (RP) is the irreal element of the complex power that is stored as magnetic and electric fields in inductors and capacitors [1]. RP is necessary for transferring useful energy in an alternating current (AC) system since it enables maintaining voltage stability in an electric power system (EPS). Although this is an important aspect of power flow, it is considered an important barrier to obtaining quality power and a constant voltage [2]. Many devices exchange (absorb or inject) reactive power with the electrical network, such as inductive loads, load peaks, energy theft, or the connection of various generation units to the distribution network. Therefore, during regular daily operations, the voltage in various buses across the system increases or decreases. The voltage at the receiving end depends on the reactive power within the system. Hence, appropriate voltage control and reactive power compensation are required to regulate the system voltage and reduce active power losses [3–12].

Reactive power control leads to an improvement in the performance of AC supply systems. Compensation has two important aspects, namely, load compensation and voltage support. In this sense, load compensation addresses various issues such as power factor, real power equilibrium, and voltage regulation and eliminates system harmonics. On the other hand, voltage support reduces voltage variation at any end of the transmission line [13]. As such, reactive power (VAR) compensation promotes the stability of the AC system, since it increases the maximum level of active power that may be transferred.

In contrast, FACTS controllers provide an excellent capability to regulate the alternating current (AC) supply since they increase or decrease power flow in a specific line and respond almost instantaneously to stability issues [14]. A flexible alternating current transmission system (FACTS) is a static device used to transmit alternating current. The

device enables us to increase maximum transmission power and improves power management capability. FACTS devices are based on power electronics and are of two types, series and parallel [15].

To address power system problems regarding voltage stability, FACTS devices may be installed at different locations of the EPS [16]. A FACTS device may be located at any bus or line of the system, but its performance varies depending on the location [17]. As such, in order to maximize the general performance of the system and guarantee an appropriate investment in FACTS devices, it is necessary to define the optimal position and size of these devices to provide effective control of the variables of interest [18].

The selection of the optimal location and size is based on economic feasibility, security, reliability, availability perspective, and supply quality. In this sense, various authors have proposed studies that help to optimize the problem of placing FACTS devices [19].

A moth flame (GBO-MFO) metaheuristic method is proposed in [20] to optimize the placement of three FACTS units (SVC, TCSC, and TCPS). In addition, additional objective functions are considered to minimize production costs and reduce power losses, as well as reduce costs and losses in the case of uncertain demand [21,22]. In this sense, hybrid gradient (GBO) and GBO-MFO optimization algorithms are used for the optimization. The test system was used to verify the effectiveness of this method in the IEEE 30-bus model.

A metaheuristic optimization technique is presented in [23] for an electric network that consists of stochastic resources of renewable energy and FACTS devices. In this sense, the profiles of renewable energy resources (photovoltaic and wind) are generated based on the stochastic probability prediction model. Similarly, the new metaheuristic optimization techniques proposed in the study are the marine predator algorithm (MPA), jellyfish search (JS), slime mold algorithm (SMA), and artificial ecosystem-based optimization (AEO). These techniques are compared with a common metaheuristic optimization such as particle swarm optimization (PSO), to address different optimal power flow (OPF) problems under different power operation scenarios. The objective functions used in the study seek to reduce the generation cost, energy losses, and voltage deviation in the power network. In addition, the system proposed is used in the IEEE 30-bus test model.

A methodology to improve the voltage profile through the ideal placement of SVC devices is described in [24]. Consequently, the SVC device is modeled mathematically in the Newton–Raphson power flow problem. In this way, the voltage profiles and flows through lines are quantified to determine the power losses before and after the ideal placement of the SVC devices. The effectiveness of the system is verified in the IEEE 9-bus and 30-bus systems.

Optimal placement of SVC and STATCOM on the EPS is carried out in [25]. For this purpose, the lighting attachment procedure optimization (LAPO) algorithm is determined. In this algorithm, the candidate buses, which are considered the most appropriate buses to be connected with the compensation devices, are determined based on the loss sensitivity indices (LSI). This step is necessary to reduce the search space and the computation time. Then, the LAPO is applied to calculate the best size and to determine the appropriate type of compensation devices in parallel with the EPS. The results are compared with modern optimization techniques, such as teaching–learning-based optimization (TLBO), genetic algorithms (GA), and PSO optimization, to confirm the applicability of the proposed technique. In addition, the test models are the 14 and 30-node systems.

An exhaustive review of optimal placement and dimensioning of the distribution static compensator (DSTATCOM) is conducted in [26]. For this purpose, the study used various approaches, such as analytical methods, artificial neural networks (ANNs), and metaheuristic methods, combined with sensitivity approaches, such as the voltage stability index and the power loss index, to choose the optimal placement and size of the DSTATCOM.

A review of multiple FACTS devices is presented in [2], which focuses on various metaheuristic optimization approaches for optimal placement and size.

Voltage stability is defined as the capability of the system to preserve the nominal voltage at all nodes close to the normal operating condition after a failure has occurred [27].

Voltage instability in the system is due to an insufficient reactive supply source or to an unnecessary reactive power absorption, which leads to voltage collapse, especially when the system is highly loaded. At this point, the system is not able to hold the generation and network programming, and thus reactive power support is key to preserving the voltage stability of the system.

Voltage stability indices (VSI) are defined as indicators to detect voltage collapse points in an EPS. VSIs are capable of identifying weak lines and buses in the network, both in offline and online modes, through phasor measuring units or static analysis, which provide information about the stability of the line connected between two nodes for different loading conditions. These are useful for determining the optimal placement and size of FACTS devices. Similarly, VSIs are a real-time indicator to determine the instability related to the voltage through the wide-area measurement system and phasor measurement unit (PMU-WAMS) [28]. The evaluation of voltage stability for a given EPS involves two elements, namely, the proximity indicated by the closeness to voltage instability and the instrument that contributed to the voltage instability. In addition, the key factors that contribute to instability are the weak voltage zones and the areas involved [29]. The proximity provides an indicator for voltage reliability, whereas the mechanism provides valuable documentation about how to prevent voltage instability for new system adaptations or operational approaches.

Voltage stability studies may be analyzed using different approaches, either static or dynamic [30]. Although voltage stability is a dynamic phenomenon, studies may be conducted using simulations of transient stability or extended medium term. Nevertheless, these activities do not provide documentation about susceptibility or stability level; in addition, they require a long time since they need to be tested under different system conditions in multiple contingency scenarios, which may be carried out using steady-state analysis [31]. Static voltage stability approaches are based on the model of steady-state analysis, which is based on the power flow equation, or the linearized dynamic model described by the steady state.

Classification of procedures for static voltage stability analysis is based on the main idea of VSI formulation, the maximum power that can be transferred through a single line, the existence of solutions for the voltage equation, PV curve, Lyapunov stability theory, Jacobian matrix, and maximum power transfer theorem [32].

In [33], the VSI classification is based on system variables, Jacobian matrix, and PMU (observability and local measurement). However, it is preferable to classify VSIs based on their type, namely, line VSI, node VSI, and general VSIs [34].

This study proposes to address the voltage stability problem through the suitable placement of SVC devices, considering the LVSI index. For this purpose, an OPF is calculated to obtain the power flows through the lines, to further divide the EPS into multiple subsystems. In order to divide the EPS, the Jacobian matrix of the system is analyzed, from which the sensitivity matrix and the table of electric distances are obtained.

The latter represents the degree of coupling between the system buses, and it is used to create multiple groups, where the strongly coupled nodes are grouped according to the physical connection of the system. In this sense, the technique used for such grouping is the fuzzy c-means clustering algorithm.

Then, the LVSI stability index is quantified in each group, and the optimization function based on the SVC implementation cost is formulated to obtain the best position of the device in each group.

2. Materials and Methods

The objective of the optimal power flow (OPF) is to determine the output dispatches of active and reactive power for each generation unit in a system where it is required to supply power to all the loads at a minimum cost while simultaneously honoring the technical constraints of the network [35].

Based on the above, it is deduced that the voltage magnitudes should be at acceptable levels of operation across the entire network. Moreover, the capacity limits of the transmission lines should be honored.

In the OPF, the dispatch of active and reactive power is determined with the purpose of reducing the energy fare; however, it is possible to consider different objectives, such as minimizing the active power losses in the network. One of the key constraints that should be considered in the OPF is the balance of active and reactive power (Equation (1)) across the system nodes [36].

$$\sum_{g \in \Omega_i} P_g - \sum_{d \in \Delta_i} L_d^P = \sum_{k \in \Lambda_i} P_{ik}(\cdot) \tag{1}$$

The active power output of generation unit g is called P_g , whereas the set of units located at node i is represented as Ω_i . The active power of load d is denoted as L_d^P , the group of demands at bus i is represented as Δ_i , and $P_{ik}(\cdot)$ refers to the active power transmitted from node i to node k through transmission line ik . At last, Λ_i refers to the set of nodes connected directly to node i through a transmission line. Another important aspect is the balance of reactive power (Equation (2)) at every node of the network.

$$\sum_{g \in \Omega_i} q_g - \sum_{d \in \Delta_i} L_d^Q = \sum_{k \in \Lambda_i} q_{ik}(\cdot) \tag{2}$$

The reactive power at the output of generation unit g is denoted as q_g , whereas L_d^Q refers to the reactive power at load d ; similarly, $q_{ik}(\cdot)$ corresponds to the reactive power transmitted from node i to node k through transmission line ik . On the other hand, in the OPF it is necessary to find the reactive power that flows between nodes $i - k$ (Equation (3)) through transmission line ik .

$$p_{ik}(\cdot) = v_i^2 Y_{L_{ik}} \cos(\theta_{L_{ik}}) - v_i v_k Y_{L_{ik}} \cos(\delta_i - \delta_k - \theta_{L_{ik}}) + \frac{1}{2} v_i^2 Y_{S_{ik}} \cos(\theta_{S_{ik}}) \tag{3}$$

The voltage magnitudes at nodes i and k are denoted as v_i and v_k , whereas $Y_{L_{ik}}$ and $Y_{S_{ik}}$ refer to the admittance in parallel and in series, respectively, of transmission line ik . Similarly, the reactive power q_{ik} that flows through nodes $i - k$ should be calculated (Equation (4)).

$$q_{ik}(\cdot) = -v_i^2 Y_{L_{ik}} \sin(\theta_{L_{ik}}) - v_i v_k Y_{L_{ik}} \sin(\delta_i - \delta_k - \theta_{L_{ik}}) - \frac{1}{2} v_i^2 Y_{S_{ik}} \cos(\theta_{S_{ik}}) \tag{4}$$

Now, it is necessary to consider that any generation unit g with the capability of producing active power must honor a lower and an upper limit (Equation (5)).

$$P_g^{min} \leq P_g \leq P_g^{max} \tag{5}$$

The minimum limit of active power generation is denoted as P_g^{min} , whereas the maximum limit is represented as P_g^{max} .

Similarly, any generation unit that is online is able to produce reactive power honoring a lower and an upper limit (Equation (6)).

$$Q_g^{min} \leq q_g \leq Q_g^{max} \tag{6}$$

The minimum limit of reactive power generation is denoted as Q_g^{min} , whereas the maximum limit is represented as Q_g^{max} .

It is also necessary to calculate the apparent power (Equation (7)) that flows from node i to node k through transmission line ik .

$$S_{ik}(\cdot) = +\sqrt{p_{ik}(\cdot)^2 + q_{ik}(\cdot)^2} \tag{7}$$

Similarly, the limit of the apparent power (Equation (8)) transmitted through the power transmission lines should be considered. This limit is related to the thermal capacity of the line conductors.

$$+ \sqrt{p_{ik}(\cdot)^2 + q_{ik}(\cdot)^2} \leq S_{ik}^{max} \quad (8)$$

The limit of the apparent power that circulates through the power transmission lines is denoted as S_{ik}^{max} . On the other hand, it is necessary to consider the upper (V_i^{min}) and lower (V_i^{max}) limits of the magnitude of voltage v_i (Equation (9)).

$$V_i^{min} \leq v_i \leq V_i^{max} \quad (9)$$

In this context, the limits of the angles of voltage (Equation (7)) and reference node (Equation (8)) are established (Equation (8)).

$$\begin{aligned} -\pi &\leq \delta_i \leq \pi \\ \delta_i &= 0 \end{aligned} \quad (10)$$

At last, the objective function (Equation (9)) enables us to find the active and reactive power produced by each generation unit, while honoring the aforementioned constraints.

$$\sum_g C_g \cdot p_g \quad (11)$$

The marginal production cost for each active power generation unit is denoted as C_g .

Flexible AC transmission systems (FACTS)

FACTS are devices that include power electronics and static controllers designed to increase performance and improve EPS control.

The main technology of FACTS is the power semiconductors since they enable a fast response compared to electromechanically switched systems. On the other hand, FACTS are capable of modulating the injection of reactive power, which is used for stabilizing the EPS after a significant disturbance; in addition, some controllers are capable of injecting active power to dampen the system.

Consequently, FACTS are useful to address problems related to the dynamic or transient stability limits of the EPS, and they are also used if a system that controls mechanical power or a system that controls active power flow has a limited duty cycle.

Static var compensator (SVC)

It is a static reactive power generator connected in parallel with the load, where the output is adjusted to exchange capacitive or inductive current for preserving or handling a specific variable of the EPS. In general, the control variable in the EPS is the voltage at the end node [37]. The SVCs have two popular configurations. The first consists of a fixed capacitor (FC) and a thyristor-controlled reactor (TCR), whereas the second consists of a thyristor-switched capacitor (TSC) and a TCR. At the limit of the minimum or maximum susceptance, the SVC behaves as a fixed capacitor or an inductor. In addition, the selection of the appropriate size is one of the important issues in the application of SVCs with respect to the improvement of voltage stability [38].

Ideal location of the SVC

The ideal location of this type of device is related to the installation cost. In other words, the installation of SVC devices at all nodes of the EPS implies very high costs. Therefore, it is necessary to find the optimal place within the EPS. For this purpose, it is necessary to estimate the installation cost according to the reactive power (Equation (10)) [39].

$$C_{SVC} = 0.0003Q_k^2 - 0.3051Q_k + 127.38 \quad (12)$$

For this purpose, Q_k refers to the reactive power capacity of the installed SVC, given in Mvar. Similarly, the installation cost of an SVC device with low capacity implies a high cost, as opposed to a high-capacity unit, which has low installation costs (Figure 1). As

it is a quadratic function, it can be observed that the lowest installation costs appear in capacities close to 500 Mvar. An increase in the price of installing the SVC device occurs for capacities lower or higher than this value.

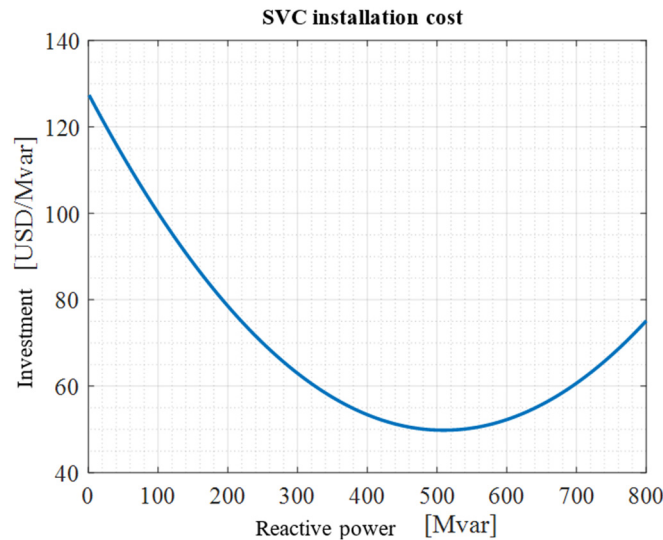


Figure 1. SVC cost function.

Representative zones in the EPS

The technical approach is based on the PV curve method in conjunction with modal analysis. For this purpose, a system space of operation is defined based on a broad range of loading conditions, dispatch conditions, and defined transactions. Then, a comprehensive set of contingencies that cover a variety of credible threats is established. Consequently, using the PV curves, the system is driven through each condition under all contingencies until the point of voltage instability is found [40].

In this manner, the voltage control area (VCA) is identified for each case using modal analysis. In this sense, at the point of instability, a modal analysis is performed by means of the PV curve to determine the critical mode, which is defined by a set of participation factors of the node corresponding to the eigenvalue [41].

The results of the modal analysis are collected in a data bank for their further analysis using data mining methods, with the purpose of identifying the VCAs of the EPS.

At the same time, there are requirements of the reactive reserve to select the VCAs. This makes reference to the relationship between the concept of Q - V sensitivity and modal analysis. This is useful to determine the zone prone to voltage instability. Therefore, the network constraints are expressed in the following model linearized around the given operation point (Equation (11)) [42].

$$\begin{bmatrix} \Delta P \\ \Delta Q \end{bmatrix} = \begin{bmatrix} J_{P\theta} & J_{PV} \\ J_{Q\theta} & J_{QV} \end{bmatrix} \begin{bmatrix} \Delta\theta \\ \Delta V \end{bmatrix} \quad (13)$$

Here, ΔP refers to the incremental variation in the real power of the node, ΔQ is the gradual variation of the bus reactive power, $\Delta\theta$ corresponds to the gradual transition in the voltage angle, ΔV represents the progressive transition of the voltage level, and $J_{P\theta}$, J_{PV} , $J_{Q\theta}$, and J_{QV} are Jacobian submatrices.

The components of the Jacobian array provide the sensitivity between the power flow and the variations in the node voltage. Although both P and Q affect voltage stability to a certain extent, the main interest is the dominant relationship between Q and V . Therefore, at each operation point, a continuous P must be maintained, and the voltage stability must be evaluated, taking into account the gradual relationship between Q and V . Based on

the previous consideration, the incremental relationship between Q and V is expressed by means of Equation (12), considering that ΔP is equal to 0 [43].

$$\Delta Q = J_R + \Delta V \tag{14}$$

$$J_R = \left[J_{QV} - J_{Q\theta} J_{P\theta}^{-1} J_{PV} \right] \tag{15}$$

$$\Delta V = J_R^{-1} * \Delta Q \tag{16}$$

$$J_R^{-1} = \left[\frac{\partial V}{\partial Q} \right] \tag{17}$$

In this case, J_R is the reduced Q - V Jacobian submatrix. Similarly, J_R^{-1} is the Q - V sensitivity array. Likewise, the i -th element in the diagonal of matrix J_R^{-1} is the Q - V sensitivity at bus i , which assumes the slope of the Q - V curve at a specific operating point. In this context, a positive Q - V sensitivity requires an invariant operation, i.e., a smaller sensitivity results in a more stable system. This is due to the fact that the sensitivity becomes infinity at the limit of stability. In addition, J_R^{-1} is a whole matrix whose elements correspond to the expansion of the voltage difference across the system after a supply of reactive power in the bus [44].

Inspection of Q - V sensitivity

The Q -sensitivity provides information about the combined effects of all the fluctuation modes of the reactive power with respect to the voltage. The relationship between the Q - V sensitivities of the buses and the eigenvalues may be derived from Equation (15). Then, Equation (16) is obtained using the variables and the bi-dimensional arrays from the reduced Jacobian J_R [45].

$$J_R = \zeta \Lambda \eta \tag{18}$$

Here, $\zeta = [\zeta_1, \zeta_2, \dots, \zeta_N]$ is the matrix of the right eigenvector of J_R , $\eta = [\eta_1, \eta_2, \dots, \eta_N]$ is the array of the left eigenvector of J_R , and Λ is the matrix of eigenvalues.

$$J_R^{-1} = \zeta \Lambda^{-1} \eta \tag{19}$$

$$\Delta V = \zeta \Lambda^{-1} \eta * \Delta Q \tag{20}$$

$$\Delta V = \sum_i \frac{\zeta_i \eta_i}{\lambda_i} * \Delta Q \tag{21}$$

In the equations above, λ_i is the i -th eigenvalue of J_R , and ζ_i and η_i are the corresponding right and left eigenvectors. The Q - V bus sensitivities may be derived from Equation (19). For this purpose, $\Delta Q = e_k$, where e_k has all elements equal to zero except factor k , which is equal to 1. Thus, the Q - V sensitivity at bus k is given by Equation (20).

$$\frac{\partial V_k}{\partial Q_k} = \sum_i \frac{\zeta_{ki} \eta_{ki}}{\lambda_{ki}} \tag{22}$$

In this case, ζ_{ki} and η_{ki} are the k -th elements of the right and left eigenvectors corresponding to the eigenvalue λ_i .

The Q - V sensitivities provide information about the combined effects of all modes in the variation of the reactive power of the voltage. The magnitudes of the specific variables may provide a relative dimension close to voltage instability. Therefore, when the system reaches the critical point of voltage stabilization, modal analysis helps to determine the critical region of voltage stabilization and the buses involved in each busbar.

The relative participation of bus k in mode i is given by the bus participation factor (Equation (21)) [45].

$$P_{ki} = \zeta_{ki} \eta_{ki} \tag{23}$$

Creation of VCAs using fuzzy c -means

The most popular clustering method is fuzzy c-means, which is of great interest due to its fast convergence. Consequently, this strategy is used to identify the VCAs after performing the power flow and estimating the $\frac{\partial V_k}{\partial Q_k}$ sensitivity array.

The fuzzy c-means technique is based on the Euclidean distance with the addition of a membership vector, which is defined as a distance between two points that would be quantified with a rule. Therefore, in the space of dimension N , the Euclidean distance between two points P and Q is represented by Equation (22).

$$\|P - Q\| = \sqrt{(p_1 - q_1)^2 + (p_2 - q_2)^2 + \dots + (p_n - q_n)^2} \quad (24)$$

Here, $p_i - q_i$ is the coordinate of $p - q$ in dimension i . With respect to this, fuzzy c-means uses the Euclidean distance concept to measure the similarity or dissimilarity between each point of the data array and the center of the clusters. This enables us to determine the cluster to which the best point corresponds. In contrast, the technique attempts to separate the data points into an appropriate number of clusters, such that the sum of the Euclidean distances of all points of the data array to the center of the corresponding cluster is minimized [40].

Linear voltage stability indicator

This indicator is used to evaluate voltage safety based on a reduced model of the system. Therefore, the LVSI enables us to easily estimate how close or far the current system operation state is from voltage collapse because it increases linearly as the load increases. Thus, the voltage collapse will occur when the LVSI is close to one. The LVSI is determined using Equation (23) [46].

$$LVSI = \frac{d_p + d_q}{d_0} \quad (25)$$

Problem Formulation

During the operation and interruption of some lines or critical equipment, the EPS may become unsafe and vulnerable to voltage collapse and instability. This is due to the lack of reactive power support and to network overloading. In addition, generators have a limited reactive power capacity, which cannot be used effectively because generation is located far from the load. Another important aspect is that generators sometimes should reduce their real power with the purpose of fulfilling the reactive power required by the system, which leads to a loss of opportunities in the electric market. Similarly, a low-voltage scenario implies a reduction of the load. Therefore, reactive power compensators are required in the transmission regime to preserve the voltage profile and, thus, improve the steady-state and dynamic performance of the EPS.

For this reason, a clustering process of coherent nonoverlapping nodes is proposed. These clusters refer to the sets of nodes that constitute a VCA only if they are, from the electrical point of view, sufficiently disconnected from the areas close to them (Algorithm 1).

In this case, each VCA is constituted by those nodes that have an important connection or electrical dependence on each other.

Therefore, the voltage scheme of a node in any VCA is effectively managed by means of the reactive power supports in it; similarly, the controls within an area are influenced by other areas. Therefore, Algorithm 1 is used to obtain normalized electrical distances, which are useful for applying the subsequent clustering process (Algorithm 2).

Algorithm 1. Procedure for the creation of VCAs

1	Enter OPF parameters	
2	Determine OPF	
3	Quantify Jacobian array	$\begin{bmatrix} \Delta P \\ \Delta Q \end{bmatrix} = \begin{bmatrix} J_{P\theta} & J_{PV} \\ J_{Q\theta} & J_{QV} \end{bmatrix}$
4	Extract matrix J_{QV}	$J_{QV} = \frac{\partial V}{\partial Q}$
	Invert array J_{QV}	$\Delta Q = J_R + \Delta V$
5		$J_R = \begin{bmatrix} J_{QV} - J_{Q\theta} J_{P\theta}^{-1} J_{PV} \\ \Delta V = J_R^{-1} * \Delta Q \\ J_R^{-1} = \left[\frac{\partial V}{\partial Q} \right]$
	Obtain the sensitivity set $\frac{\partial V_k}{\partial Q_k}$	$J_R = \zeta \Lambda \eta$
6		$\Delta V = \zeta \Lambda^{-1} \eta * \Delta Q$
		$\Delta V = \sum_i \frac{\zeta_i \eta_i}{\lambda_i} * \Delta Q$
		$\frac{\partial V_k}{\partial Q_k} = \sum_i \frac{\zeta_{ki} \eta_{ki}}{\lambda_{ki}} = a$
7	Estimate the array of attenuations α_{ij}	$\alpha_{ij} = \frac{a_{ij}}{a_{jj}}$
8	Collect the matrix of electrical distances D_{ij}	$D_{ij} = -\log(\alpha_{ij}, \alpha_{ji})$
9	Normalize the electrical distances D_{ij}	$D_{ij} = \frac{D_{ji}}{\max(D_{i1}, \dots, D_{iN})}$

Algorithm 2. Identification of VCAs

1	Enter electrical distances D_{ij} determined using Algorithm 1
2	Arbitrarily choose k initial cluster centers $Z_1(1), Z_2(1), \dots, Z_k(1)$
	Distribute the samples $\{X\}$ among the k domains
3	Do for all r until k Si $\ x - Z_j(r)\ < \ x - Z_i(r)\ $ $x \in S_j(r)$
4	Calculate the new cluster centers $Z_j(r+1)$ Do for all j until k $Z_j(k+1) = \frac{1}{N} \sum_{X \in S_j(k)} X$
	Verify convergence
	Do for all j until k If $Z_j(r+1) = Z_j(r)$
5	Algorithm converges Print VCA Otherwise Return to Step 2

Algorithms 1 and 2 are used to obtain the VCAs in an EPS. In other words, various weakly coupled clusters are generated within the same system. These should be compensated separately, for which an optimization system is formulated based on the implementation price of SVC equipment (Algorithm 3).

Algorithm 3. Calculation of LVSI index

1	Compute OPF Obtain the equivalent sum of the load and the generation	$P_{Load} = \sum_1^n P_L$
2	Quantify d_p, d_q y d_0	$Q_{Load} = \sum_1^n Q_L$ $P_g = \sum_1^n P_g$ $Q_g = \sum_1^n Q_g$
3	Determine the equivalent impedance and the angle	$z_{eq} = R_{eq} + jX_{eq}$ $\theta \leq z_{eq}$
4	Quantify d_p, d_q y d_0	$d_p = \left E * \left(\frac{1 - \sqrt{\frac{1 - 4pr}{E^2}}}{2 * \cos(\theta)} \right) \right $ $d_q = E * \left(\frac{1 - \sqrt{\frac{1 - 4pr}{E^2}}}{2 * \sin(\theta)} \right)$ $d_0 = E * \left(\frac{\sin(\theta) + \cos(\theta) - 1}{2 * \sin(\theta) * \cos(\theta)} \right)$
5	Determine the LVSI	$LVSI = \frac{d_p + d_q}{d_0}$

Thus, the expression to optimize corresponds to the reduction of the investment cost of the SVC active in the system together with the LVSI stability indicator (Equation (24)), which is quantified through Algorithm 3. At the same time, y_j is controlled using the sum of binary variables related to the connectivity of the system (Equation (25)). Similarly, to avoid placing an SVC device in a bus with the generation, the product of the active SVC (y_j) and the connection mapping of each generator is made (Equation (26)).

$$\min \sum_{j=1}^k C_j * y_j * LVSI \tag{26}$$

$$y_j + \sum_{\substack{i=1 \\ i=j}}^k x(i) \geq 1 \tag{27}$$

$$\sum_{\substack{i=1 \\ i=j}}^k y(i) * gen(i) \leq 0 \tag{28}$$

In this case, C_j refers to the investment cost of the SVC, y_j makes reference to a binary variable that controls the activation of the compensator device, $x(i)$ corresponds to the connectivity array of the system, and $gen(i)$ is a binary array that indicates the connection node of the generator. Therefore, the proposed technique is applied to schemes of 14 (Figure 2) and 30 nodes (Figure 3).

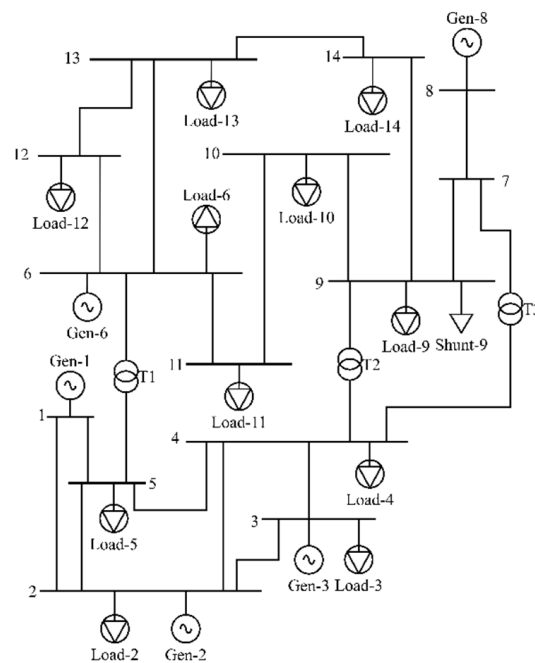


Figure 2. IEEE 14-bus test system.

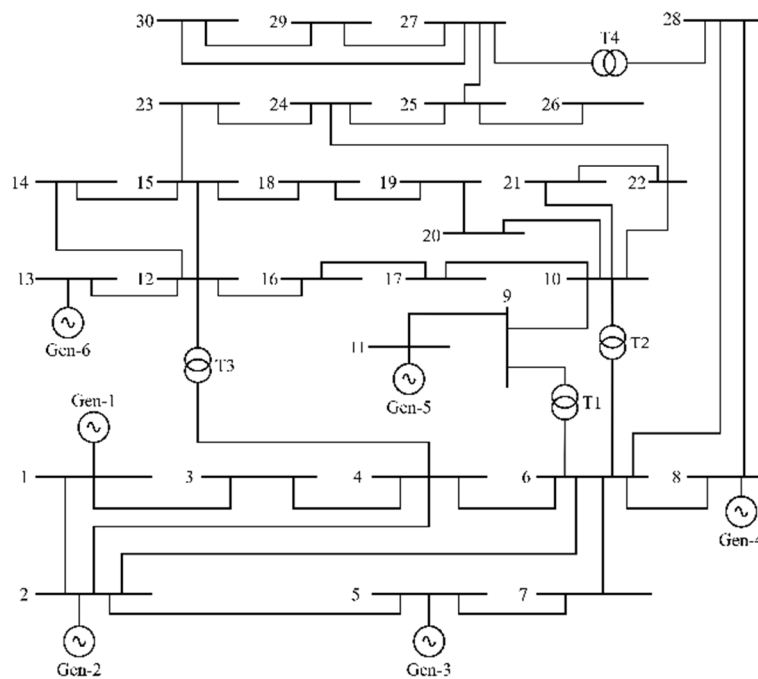


Figure 3. IEEE 30-bus test system.

3. Results

Three scenarios are presented to test the proposed technique for the ideal placement of SVC devices by means of clustering techniques and the LVSI voltage stability indicator. A different value of reactive power for the SVC device is considered in each case (1 Mvar, 3 Mvar, and 6 Mvar). Therefore, some variables are quantified in the 14-node and 30-node schemes, which include voltage profile, the behavior of the angle, power dispatch, and system losses. These variables are obtained using the proposed method and are compared with the results obtained in Power Factory.

IEEE 14-bus test system

Three clusters were created for the 14-node scheme (Table 1). The first cluster includes three nodes and one SVC device optimally placed. On the other hand, the second cluster consists of four nodes and two compensators, whereas the third cluster has seven nodes and three SVC devices (Figure 4). In addition, the LVSI for this scheme is 0.0641, which implies that the EPS is far from voltage collapse.

Table 1. Resulting VCAs for the 14-node test scheme.

VCA	Component	Placement of the SVC
1	12	-
	13	X
	14	-
2	6	-
	9	X
	10	-
3	11	X
	1	-
	2	-
	3	-
	4	X
	5	X
	7	X
8	-	

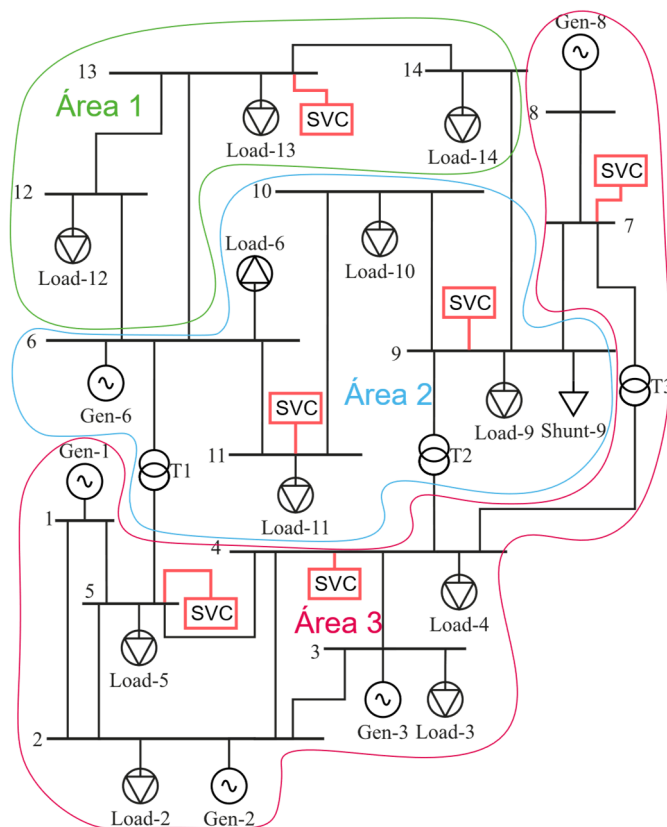


Figure 4. VCAs in the IEEE 14-bus test system.

On the other hand, the voltage profile when the SVC device is not installed reaches a magnitude of 1.06 per unit in some nodes (Figure 5). In contrast, such a profile improves significantly after the SVC devices have been installed since the maximum value reached in some nodes is 1 per unit (Figure 6).

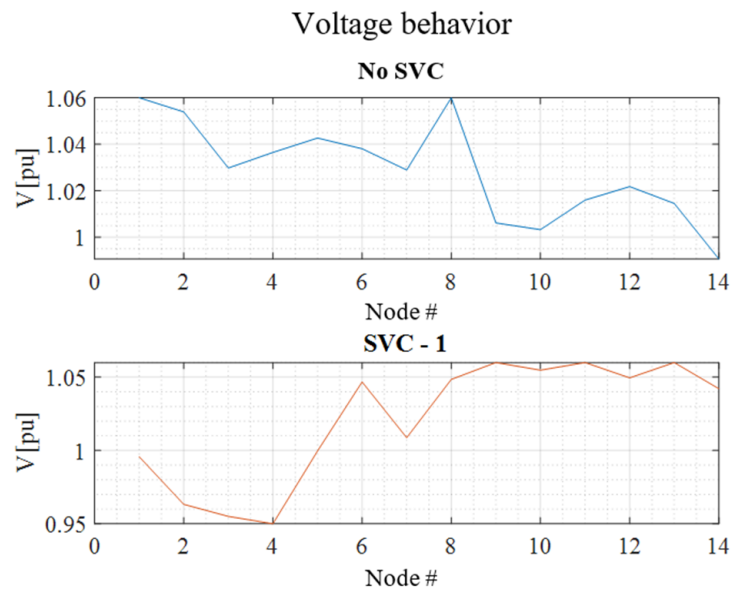


Figure 5. Voltage profile in the IEEE 14-bus test system.

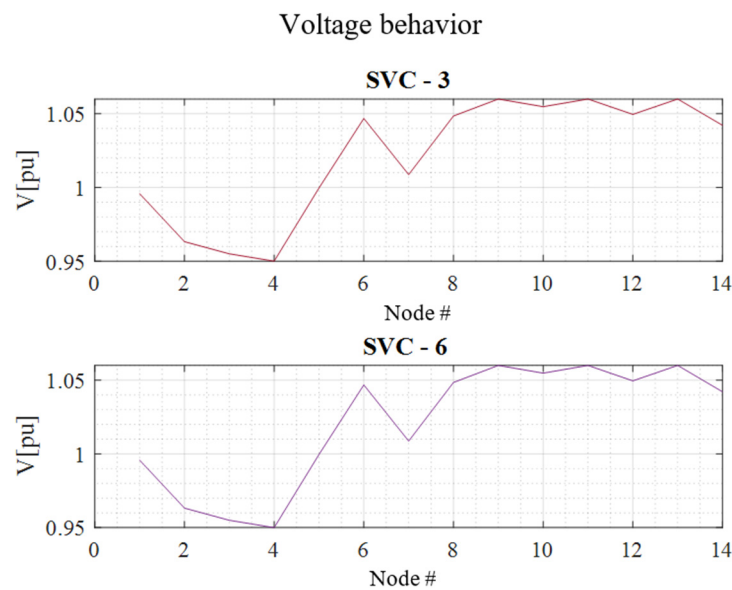


Figure 6. Voltage profile in the IEEE 14-node system: SVC 3 and 6.

In addition, the voltage profile is reorganized such that it attempts to reach a value of one. Nevertheless, it is verified that an SVC with a capacity of 1 Mvar is the one that best compensates the voltage profile since SVCs of higher capacity do not contribute to a significant improvement compared to the 1 Mvar SVC. Similarly, the system angle profile without SVC is significantly corrected when a 1 Mvar SVC is installed (Figure 7).

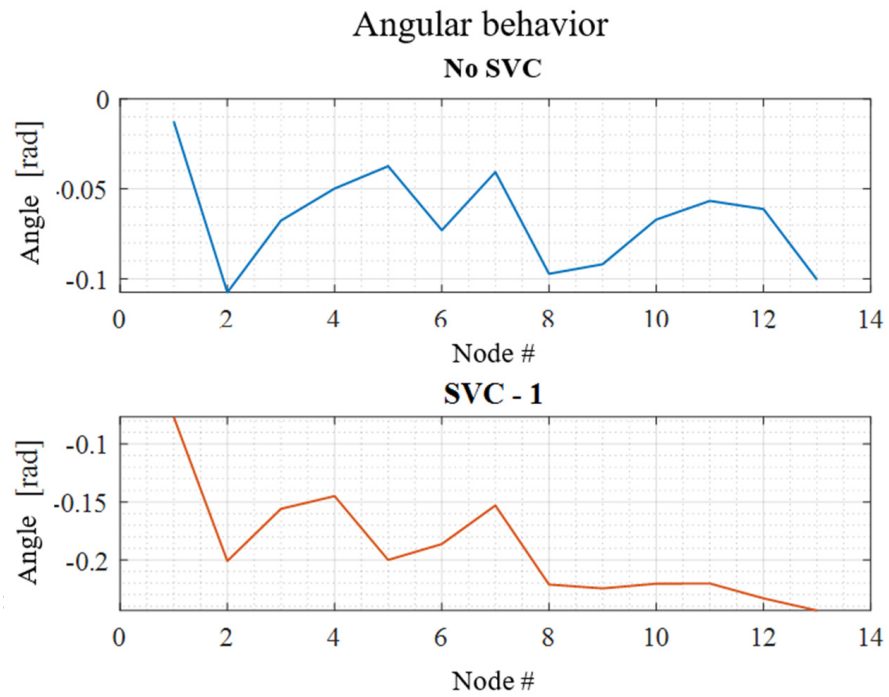


Figure 7. Angle profile in the IEEE 14-bus test system.

An essential aspect that should be mentioned is that the angle profile worsens when an SVC with a large capacity is used (Figure 8).

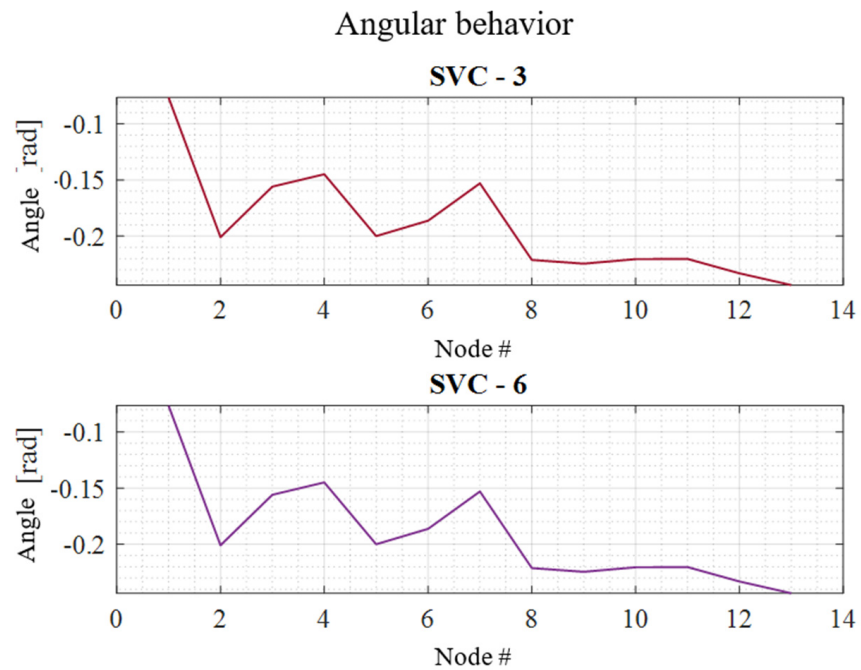


Figure 8. Angle profile in the IEEE 14-bus test system: SVC 3 and 6.

Similarly, the nodal behavior of the reactive power substantially improves with the 1 Mvar SVC compared to the base system, which has no compensator (Figure 9).

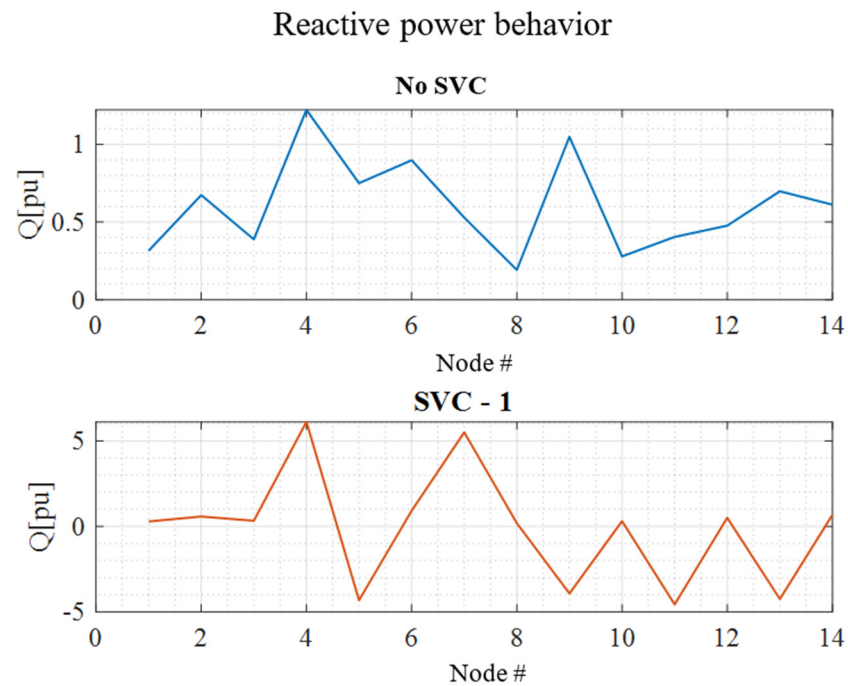


Figure 9. Profile of nodal reactive power in the IEEE 14-bus test system.

In addition, the nodal reactive power increases significantly when very high-capacity compensators are used, but this does not imply a significant improvement in the nodal voltage profile (Figure 10).

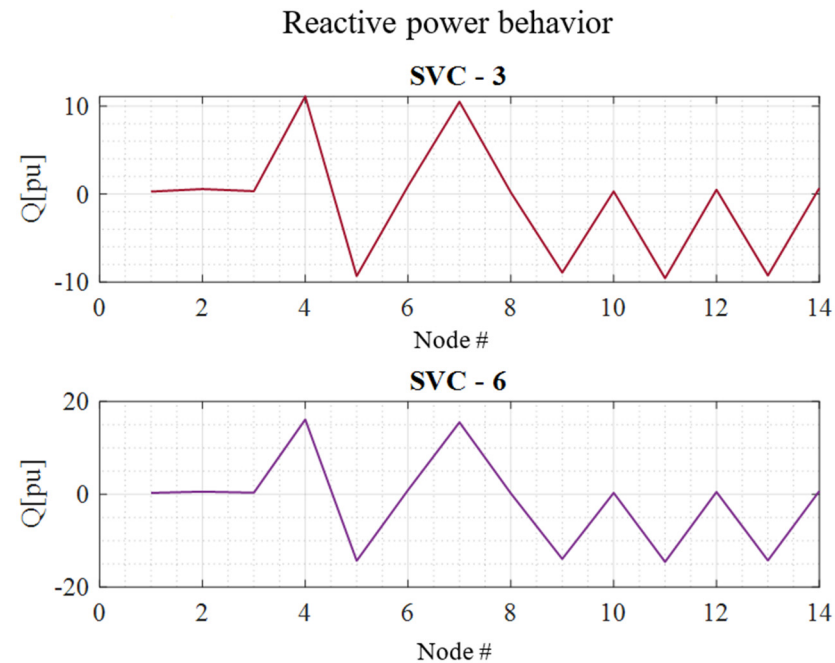


Figure 10. Profile of nodal reactive power in the IEEE 14-bus test system: SVC 3 and 6.

Similarly, the reactive power losses decrease considerably when a 1 Mvar SVC device is installed (Figure 11), but for high values of SVC, these losses increase significantly in some nodes (Figure 12).

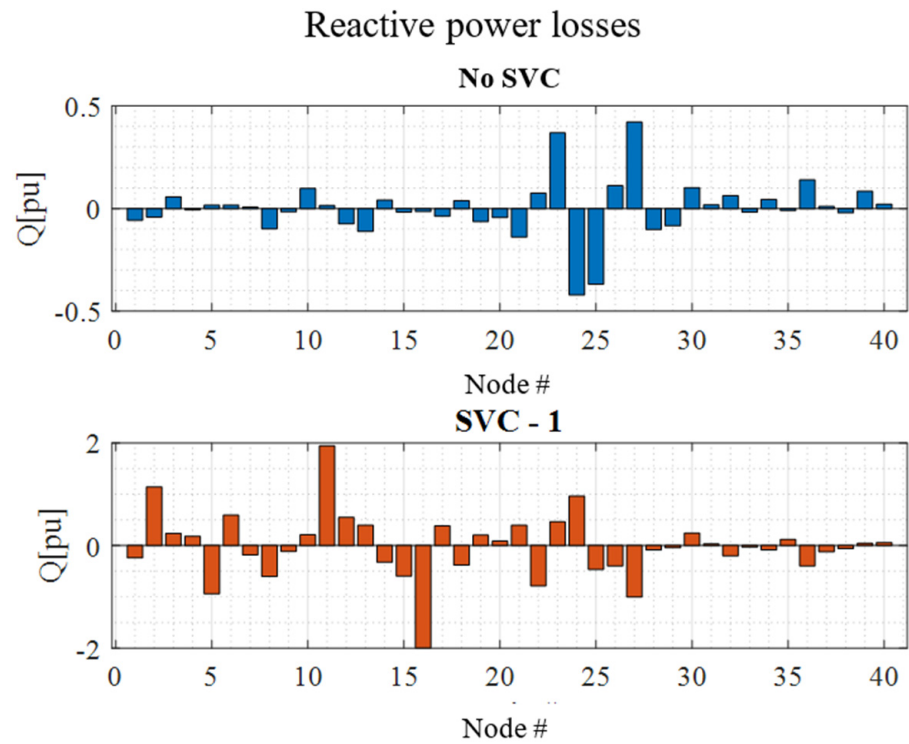


Figure 11. Profile of nodal reactive power for the IEEE 14-bus test system.

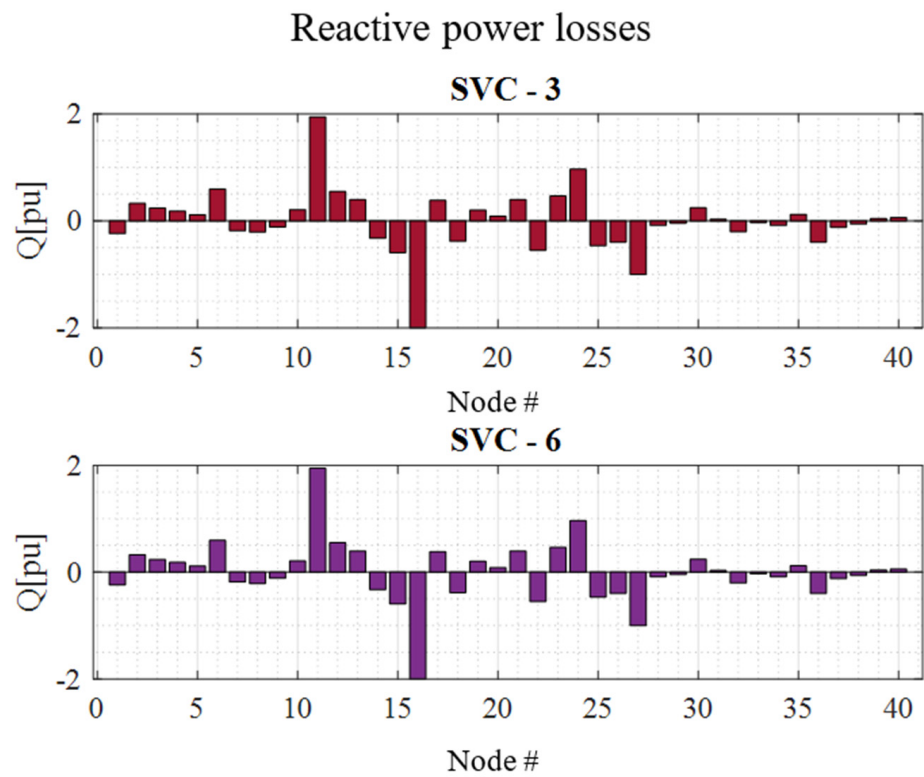


Figure 12. Profile of nodal reactive power for the IEEE 14-bus test system: SVC 3 and 6.

On the other hand, the results obtained for each scenario are compared with the ones obtained using Power Factory (Table 2).

Table 2. Comparison of the voltage profile in the 14-node scheme. GAMS vs. Power Factory.

W/O SVC		SVC (1)		SVC (3)		SVC (6)	
GAMS	Power Factory						
1.060	1.060	0.996	1.060	0.996	1.060	0.996	1.060
1.054	1.045	0.963	1.045	0.963	1.045	0.963	1.045
1.030	1.010	0.955	1.010	0.955	1.010	0.955	1.010
1.036	1.019	0.950	1.018	0.950	1.016	0.950	1.013
1.043	1.020	1.000	1.019	1.000	1.018	1.000	1.015
1.038	1.070	1.047	1.070	1.047	1.070	1.047	1.070
1.029	1.062	1.009	1.060	1.009	1.057	1.009	1.053
1.060	1.090	1.048	1.090	1.048	1.090	1.048	1.090
1.006	1.056	1.060	1.055	1.060	1.051	1.060	1.046
1.003	1.051	1.055	1.050	1.055	1.046	1.055	1.041
1.016	1.057	1.060	1.055	1.060	1.051	1.060	1.046
1.022	1.055	1.050	1.053	1.050	1.049	1.050	1.042
1.015	1.050	1.060	1.049	1.060	1.045	1.060	1.040
0.991	1.036	1.042	1.034	1.042	1.031	1.042	1.026

With respect to this, it is evident that the magnitudes obtained in this research are similar to the ones given by the commercial software, although there is a certain degree of error in some cases.

IEEE 30-bus test system

Three clusters were created for the 30-node scheme (Table 3). The first cluster includes five nodes and two SVC devices optimally placed. Similarly, the second cluster consists of 13 nodes and 5 compensators, while the third cluster has 12 nodes and 4 SVC devices (Figure 13). In addition, the LVSI for this scheme is 0.0267, which implies that the EPS is far from voltage collapse.

Table 3. Resulting VCAs for the 30-node test scheme.

VCA	Component	Placement of the SVC
1	25	-
	26	X
	27	X
	29	-
	30	-
2	12	X
	13	-
	14	-
	15	-
	16	-
	17	X
	18	-
	19	X
	20	-
	21	X
22	-	
23	-	
24	X	

Table 3. Cont.

VCA	Component	Placement of the SVC
3	1	-
	2	-
	3	X
	4	X
	5	-
	6	-
	7	X
	8	-
	9	X
	10	-
	11	-
	28	-

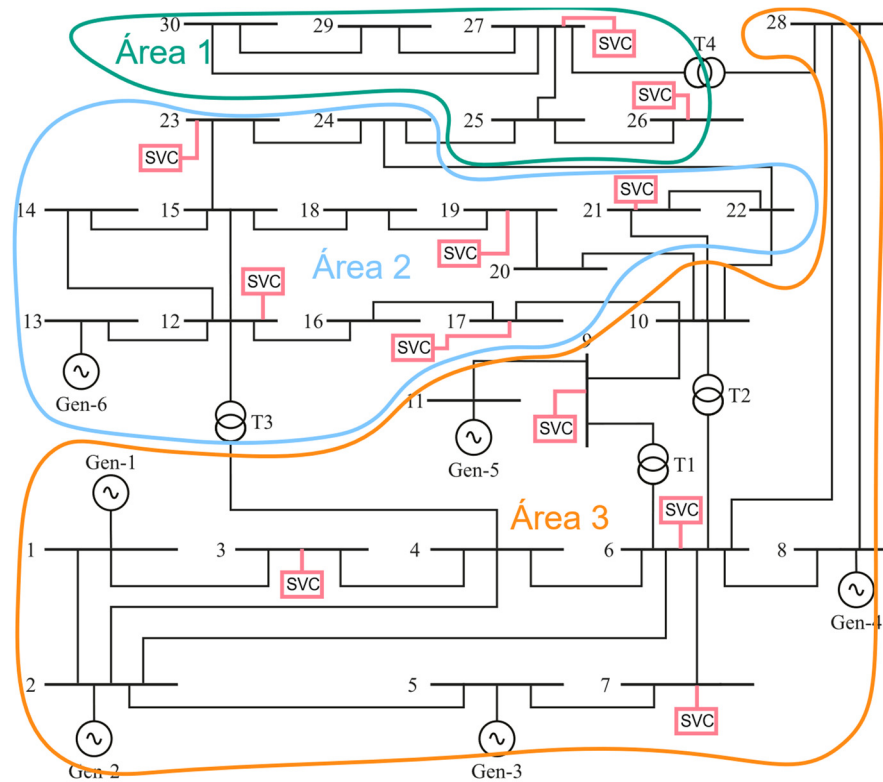


Figure 13. VCAs in the IEEE 30-bus test system.

On the other hand, when no SVC device is installed, the voltage profile reaches a magnitude of 1.06 per unit in some nodes (Figure 14). In contrast, the voltage profile significantly improves when SVC devices are installed since the maximum magnitude obtained in some nodes is 1 per unit (Figure 15).

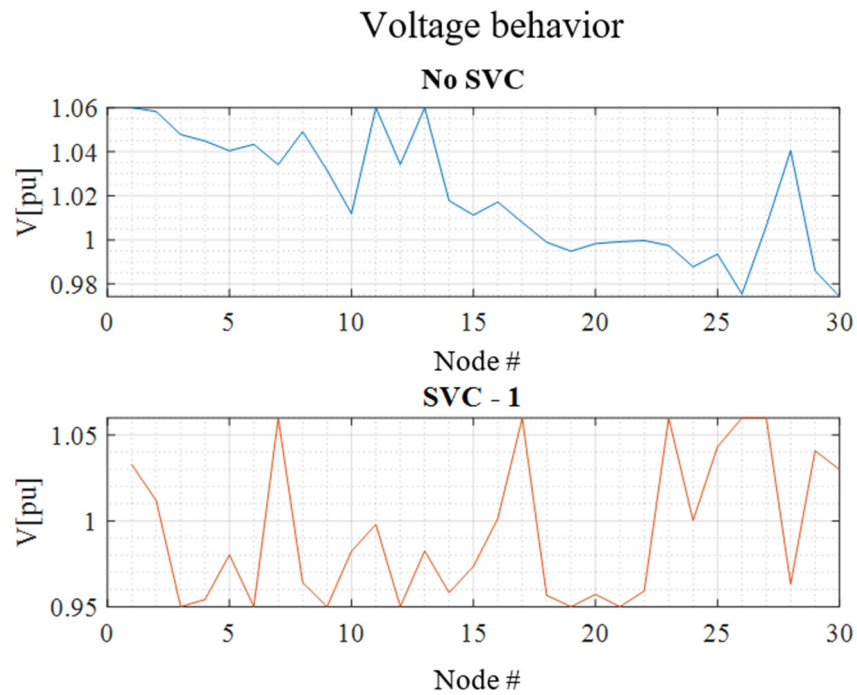


Figure 14. Voltage profile in the IEEE 30-bus test system.

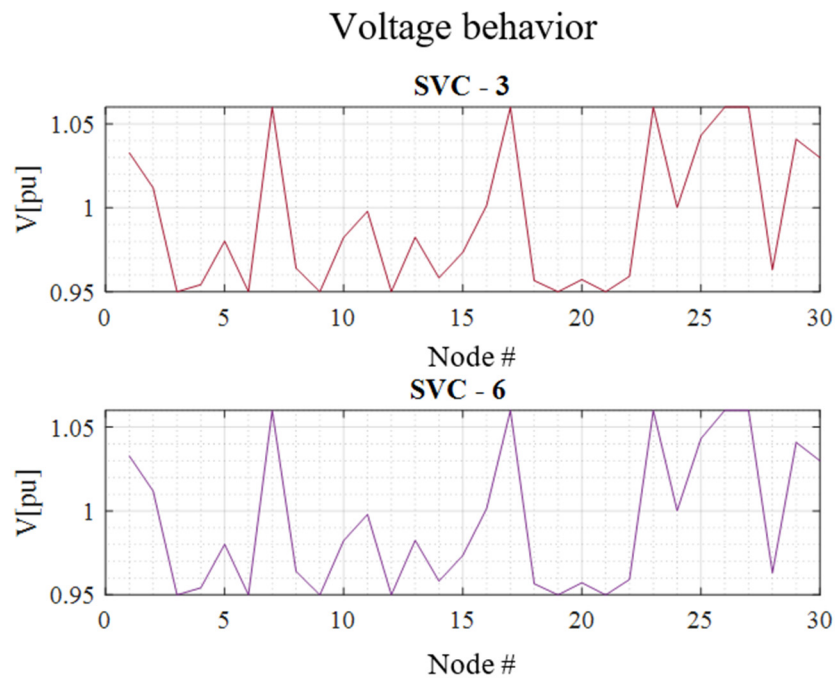


Figure 15. Voltage profile in the IEEE 30-bus test system: SVC 3 and 6.

In addition, the voltage profile is reorganized such that it attempts to reach a value of one. Nevertheless, it is verified that an SVC with a capacity of 1 Mvar is the one that best compensates the voltage profile since SVCs of higher capacity do not contribute a significant improvement compared to the 1 Mvar SVC.

Similarly, the system angle profile without SVC is significantly corrected when a 1 Mvar SVC is installed (Figure 16). An essential aspect that should be mentioned is that the angle profile worsens when an SVC with a large capacity is used (Figure 17).

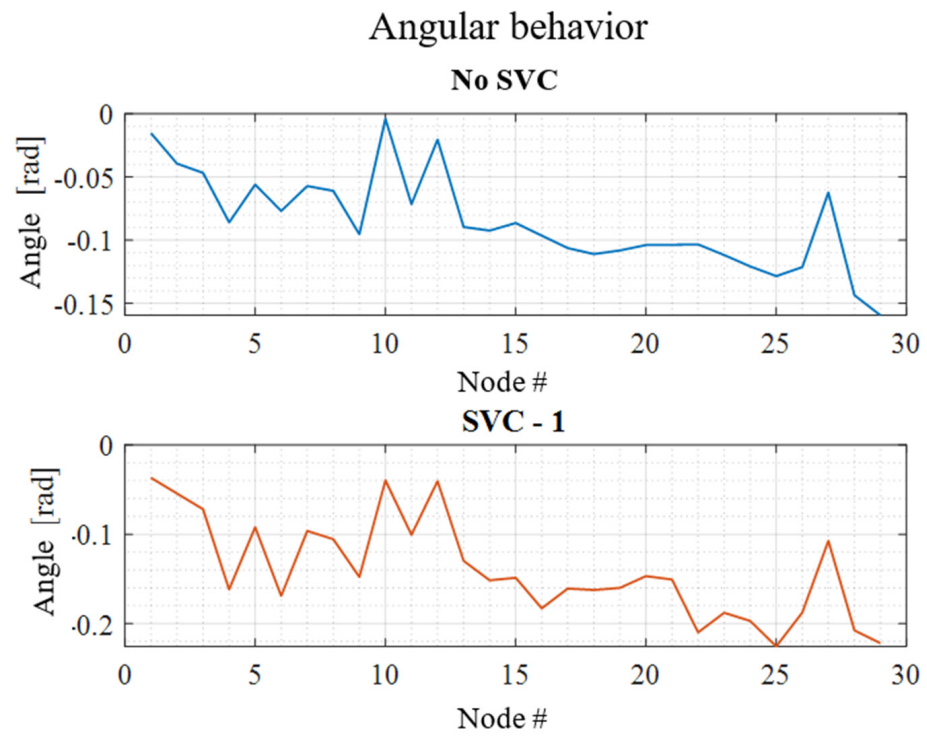


Figure 16. Angle profile in the IEEE 30-bus test system.

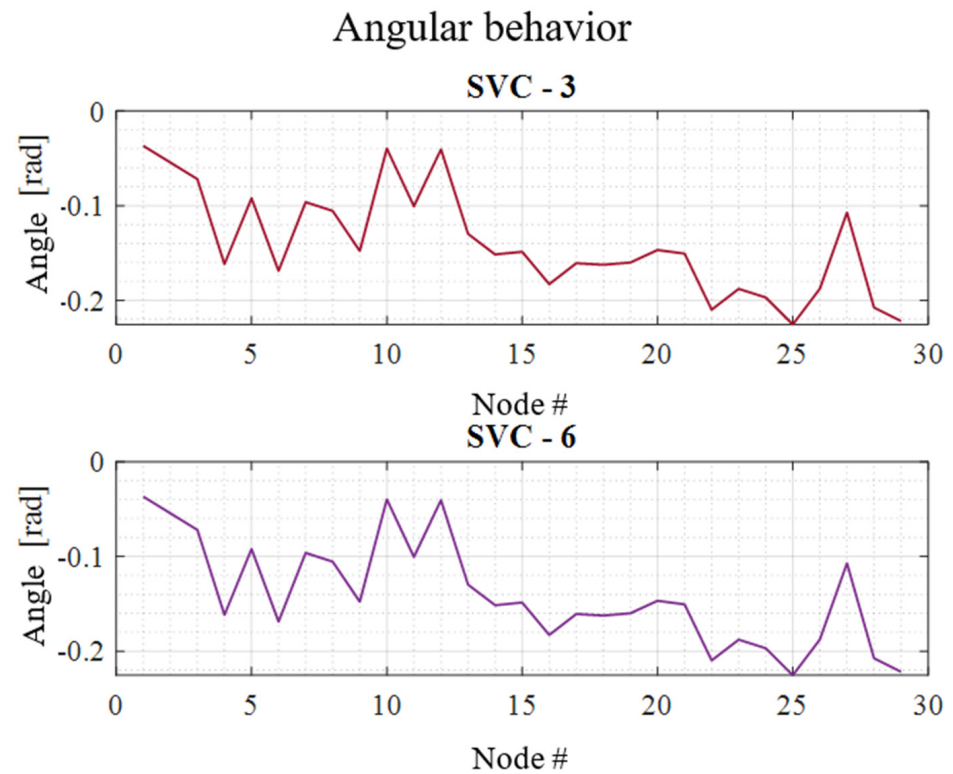


Figure 17. Angle profile in the IEEE 30-bus test system: SVC 3 and 6.

Similarly, the nodal behavior of the reactive power substantially improves with the 1 Mvar SVC compared to the base system with no compensator (Figure 18).

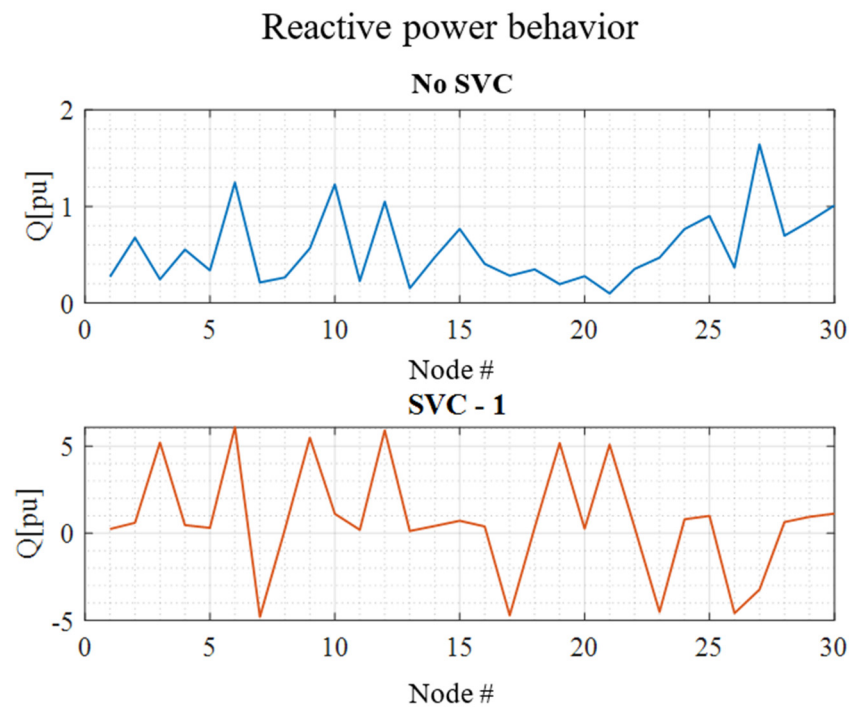


Figure 18. Profile of nodal reactive power in the IEEE 30-bus test system.

In addition, the nodal reactive power increases significantly when very high-capacity compensators are used, but this does not imply a significant improvement in the nodal voltage profile (Figure 19).

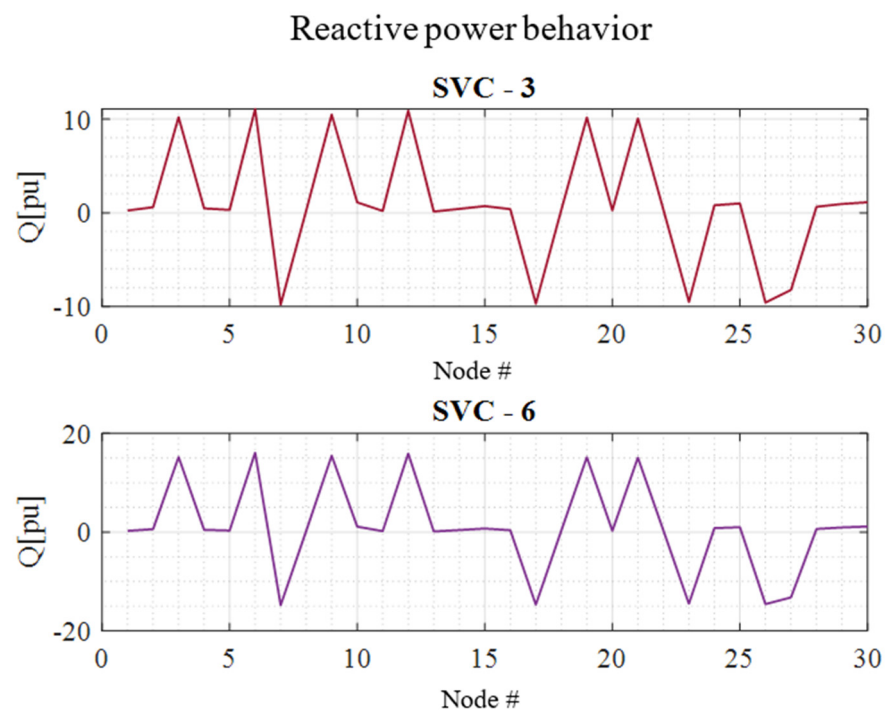


Figure 19. Profile of nodal reactive power in the IEEE 30-bus test system: SVC 3 and 6.

Similarly, the reactive power losses decrease considerably when a 1 Mvar SVC device is installed (Figure 20), but for high values of SVC, these losses increase significantly in some nodes (Figure 21).

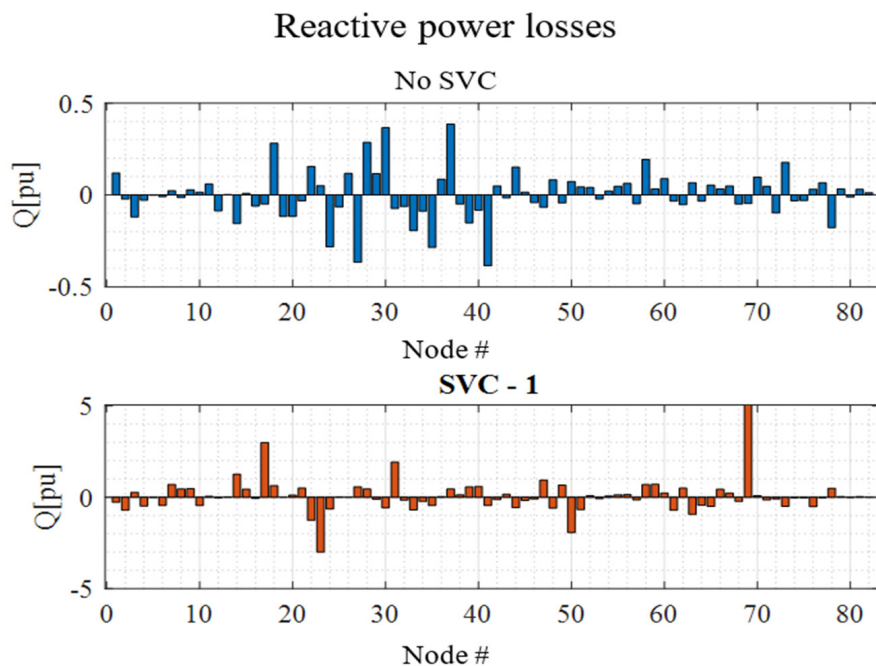


Figure 20. Profile of nodal reactive power for the IEEE 30-bus test system.

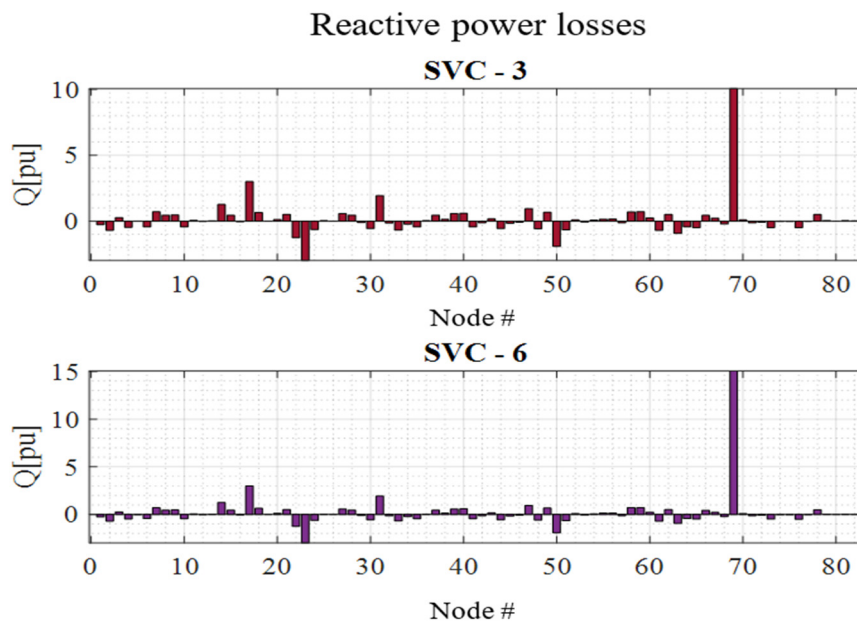


Figure 21. Profile of nodal reactive power for the IEEE 30-bus test system: SVC 3 and 6.

In this case, it is evident that the magnitudes obtained in this research are similar to the ones given by the commercial software, although there is a certain degree of error in some cases.

Finally, when the data obtained in this research are compared with the study proposed in [36], it is concluded that the technique proposed is effective, since the SVC devices are also placed efficiently in the aforementioned study.

The study proposed in [36] presents an approach to ideally place SVC with the purpose of improving the voltage profile. In this sense, it employs the L_j voltage stability index. This indicator varies between zero and one, such that a magnitude closer to one implies that the EPS is very close to voltage instability.

Compared to the previously described study, the results obtained in this research are very similar, considering the LVSI stability indicator.

Table 4 shows a comparison of the voltage profile in the 30-node scheme (GAMS: Power Factory).

Table 4. Comparison of the voltage profile in the 30-node scheme. GAMS vs Power Factory.

W/O SVC		SVC (1)		SVC (3)		SVC (6)	
GAMS	Power Factory						
1.060	1.060	1.033	1.060	1.033	1.060	1.033	1.060
1.058	1.000	1.012	0.995	1.012	0.987	1.012	0.975
1.048	1.082	0.950	1.082	0.950	1.082	0.950	1.082
1.045	1.025	0.954	1.022	0.954	1.017	0.954	1.010
1.040	1.071	0.980	1.071	0.980	1.071	0.980	1.071
1.043	1.008	0.950	1.004	0.950	0.998	0.950	0.989
1.034	1.001	1.060	0.997	1.060	0.990	1.060	0.979
1.049	1.006	0.964	1.003	0.964	0.997	0.964	0.987
1.032	0.996	0.950	0.993	0.950	0.985	0.950	0.974
1.012	0.988	0.982	0.983	0.982	0.973	0.982	0.959
1.060	0.983	0.998	0.978	0.998	0.967	0.998	0.951
1.034	1.045	0.950	1.045	0.950	1.045	0.950	1.045
1.060	0.987	0.982	0.981	0.982	0.971	0.982	0.956
1.018	0.986	0.958	0.982	0.958	0.972	0.958	0.959
1.011	0.987	0.973	0.982	0.973	0.972	0.973	0.959
1.017	0.985	1.001	0.980	1.001	0.970	1.001	0.956
1.008	0.973	1.060	0.966	1.060	0.953	1.060	0.934
0.999	0.973	0.957	0.964	0.957	0.948	0.957	0.924
0.995	0.954	0.950	0.942	0.950	0.918	0.950	0.884
0.998	0.981	0.957	0.974	0.957	0.959	0.957	0.938
0.999	1.004	0.950	1.003	0.950	1.000	0.950	0.995
1.000	0.961	0.959	0.953	0.959	0.938	0.959	0.916
0.997	1.022	1.060	1.021	1.060	1.018	1.060	1.014
0.988	0.949	1.000	0.941	1.000	0.926	1.000	0.904
0.994	1.014	1.043	1.013	1.043	1.011	1.043	1.007
0.975	1.010	1.060	1.010	1.060	1.010	1.060	1.010
1.006	1.009	1.060	1.008	1.060	1.006	1.060	1.003
1.041	1.001	0.963	1.000	0.963	0.998	0.963	0.994
0.986	1.010	1.041	1.010	1.041	1.010	1.041	1.010
0.974	1.023	1.030	1.020	1.030	1.016	1.030	1.009

4. Discussion

Although the study presented achieved the ideal placement of SVC devices in the EPS, the number of compensators considered is limited since only one device was used. Therefore, as a future work, we suggest using the same proposed technique but with a larger number of devices, such as the STATCOM. Similarly, some indices may be considered, such as the voltage stability indicator (L-index), with the purpose of supplementing the

criteria used in the research. In this manner, the effectiveness and precision of the proposed method could be improved.

5. Conclusions

This research has presented a method based on the fuzzy c-means clustering technique for placing SVC in an EPS.

The criterion to identify representative candidate nodes and the centroids for each group is based on the Euclidean distance between the members of the array. For this purpose, nodes with similar features are grouped, which is further verified using the connectivity matrix; this ensures that the grouped nodes are connected with each other.

On the other hand, for the ideal placement of SVC, it is necessary to model the devices of interest by means of the nodal power injection model. In this manner, the function associated with the installation cost of the compensator in each node of the system may be used in conjunction with the LVSI voltage stability indicator. Thus, the ideal location of compensators in each VCA is obtained. In addition, the method described in this research is effective since it is coherent with the products obtained in Power Factory as well as in similar studies.

Similarly, the application of the technique described in the 30-node scheme was demonstrated to be capable of identifying the VCAs and ideally placing the SVC. This contributes to strengthening the voltage scheme since the magnitude of the nodes is close to one. Likewise, the reactive power losses are reduced significantly, but this depends on the capacity of the SVCs installed in the EPS since a very high capacity causes a larger amount of losses in the EPS without significantly improving the voltage profile.

Author Contributions: Conceptualization, C.G. and A.A.T.; methodology, C.G. and A.A.T.; software, C.G.; validation, C.G., A.A.T. and L.O.; formal analysis, C.G.; investigation, C.G., A.A.T. and L.O.; resources, C.G., A.A.T. and L.O.; data curation, C.G.; writing—original draft preparation, C.G. and A.A.T.; writing—review and editing, C.G., A.A.T. and L.O.; visualization, C.G., A.A.T. and L.O.; supervision, A.A.T.; project administration, A.A.T.; fund-ing acquisition, A.A.T. All authors have read and agreed to the published version of the manuscript.

Funding: This research received no external funding.

Institutional Review Board Statement: Not applicable.

Informed Consent Statement: Not applicable.

Data Availability Statement: Not applicable.

Conflicts of Interest: The authors declare no conflict of interest.

Abbreviations

SVC	Static VAR Compensators
EPS	Electric Power System
LVSI	Linear Voltage Stability Index
VCA	Voltage Control Areas
OPF	Optimal Power Flow
STATCOM	Static Synchronous Compensator
GAMS	General Algebraic Modeling System
IEEE	Institute of Electrical and Electronics Engineers
TCR	Thyristor-Controlled Reactor
TSC	Thyristor-Switched Capacitor

References

1. Sulaiman, M.H.; Mustaffa, Z. Optimal placement and sizing of FACTS devices for optimal power flow using metaheuristic optimizers. *Results Control Optim.* **2022**, *8*, 100145. [[CrossRef](#)]
2. Ahmad, A.A.L.; Sirjani, R. Optimal placement and sizing of multi-type FACTS devices in power systems using metaheuristic optimisation techniques: An updated review. *Ain Shams Eng. J.* **2020**, *11*, 611–628. [[CrossRef](#)]

3. Ismail, B.; Wahab, N.I.A.; Othman, M.L.; Radzi, M.A.M.; Vijayakumar, K.N.; Naain, M.N.M. A Comprehensive Review on Optimal Location and Sizing of Reactive Power Compensation Using Hybrid-Based Approaches for Power Loss Reduction, Voltage Stability Improvement, Voltage Profile Enhancement and Loadability Enhancement. *IEEE Access* **2020**, *8*, 222733–222765. [[CrossRef](#)]
4. Águila, A.; Ortiz, L.; Orizondo, R.; López, G. Optimal location and dimensioning of capacitors in microgrids using a multicriteria decision algorithm. *Heliyon* **2021**, *7*, e08061. [[CrossRef](#)]
5. Aguila Téllez, A. Optimización multicriterio de flujos de potencia reactiva en sistemas eléctricos de distribución. Tesis de Doctorado, Universidad Pontificia Bolivariana de Medellín: Medellín, Colombia, 2021; Volume 2021-06-15, p. 105.
6. Gutierrez, G.; Aguila, A.; González, D.; Ortiz, L. Optimum location and sizing of capacitor banks using VOLT VAR compensation in micro-grids. *IEEE Lat. Am. Trans.* **2020**, *18*, 465–472. [[CrossRef](#)]
7. Medina, S.M.; Aguila, A. Óptima Compensación de Potencia Reactiva en Redes de Distribución Radiales considerando periodo de diseño Optimal Compensation of Reactive Power in Radial Distribution Networks considering design period. In Proceedings of the 2019 International Conference on Information Systems and Computer Science (INCISCOS), Quito, Ecuador, 22 November 2019; pp. 108–115. [[CrossRef](#)]
8. Téllez, A.Á.; López, G.; Isaac, I.; González, J.W. Optimal reactive power compensation in electrical distribution systems with distributed resources. Review. *Heliyon* **2018**, *4*, e00746. [[CrossRef](#)]
9. Aguila, A.; Wilson, J. Technical and Economic Assessment of the Implementation of Measures for Reducing Energy Losses in Distribution Systems. *IOP Conf. Ser. Earth Environ. Sci.* **2017**, *73*, 012018. [[CrossRef](#)]
10. Munoz, F.A.C.; Tellez, A.A.; Sanchez, J.W.G. Analysis of Stability of Tension and Losses of Electric Power in Distribution Networks with Distributed Generation. *IEEE Lat. Am. Trans.* **2016**, *14*, 4491–4498. [[CrossRef](#)]
11. Tellez, A.A.; Galarza, D.F.C.; Matos, L.O. Analysis of power losses in the asymmetric construction of electric distribution systems. *IEEE Lat. Am. Trans.* **2015**, *13*, 2190–2194. [[CrossRef](#)]
12. Aguila, A. Medidas para minimizar las pérdidas de energía en circuitos de distribución. Bachelor's Thesis, Universidad de Ciego de Ávila, Ciego de Ávila, Cuba, 2010. [[CrossRef](#)]
13. Okampo, E.J.; Nwulu, N.; Bokoro, P.N. Optimal Placement and Operation of FACTS Technologies in a Cyber-Physical Power System: Critical Review and Future Outlook. *Sustainability* **2022**, *14*, 7707. [[CrossRef](#)]
14. Ababssi, N. Implementation Optimal Location of STATCOM on the IEEE New England Power System Grid (100 kV). *INASS* **2022**, *15*, 441–454. [[CrossRef](#)]
15. Shokouhandeh, H.; Latif, S.; Irshad, S.; Kamarposhti, M.A.; Colak, I.; Eguchi, K. Optimal Management of Reactive Power Considering Voltage and Location of Control Devices Using Artificial Bee Algorithm. *Appl. Sci.* **2021**, *12*, 27. [[CrossRef](#)]
16. Khoa, N.M.; Tung, D.D. Locating fault on transmission line with static var compensator based on phasor measurement unit. *Energies* **2018**, *11*, 2380. [[CrossRef](#)]
17. Zhu, X.; Dichen, L.; Wu, J. TwoStage Optimal Location Allocations of DPFC Considering Wind and Load Uncertainty. *Front. Energy Res.* **2022**, *10*, 865902. [[CrossRef](#)]
18. Tareen, W.U.K.; Aamir, M.; Mekhilef, S.; Nakaoka, M.; Seyedmahmoudian, M.; Horan, B.; Memon, M.A.; Baig, N.A. Mitigation of power quality issues due to high penetration of renewable energy sources in electric grid systems using three-phase APF/STATCOM technologies: A review. *Energies* **2018**, *11*, 1491. [[CrossRef](#)]
19. Karmakar, N.; Bhattacharyya, B. Optimal reactive power planning in power transmission system considering facts devices and implementing hybrid optimisation approach. *IET Gener. Distrib.* **2020**, *14*, 6294–6305. [[CrossRef](#)]
20. Mohamed, A.A.; Kamel, S.; Hassan, M.H.; Mosaad, M.I.; Aljohani, M. Optimal Power Flow Analysis Based on Hybrid Gradient-Based Optimizer with Moth-Flame Optimization Algorithm Considering Optimal Placement and Sizing of FACTS/Wind Power. *Mathematics* **2022**, *10*, 361. [[CrossRef](#)]
21. Orejuela, V.; Arias, D.; Aguila, A. Response of Residential Electricity Demand Against Price Signals in Ecuador. In Proceedings of the IEEE Thirty Fifth Central American and Panama Convention, No. Concapan XXXV, Tegucigalpa City, Honduras, 11–13 November 2015; pp. 373–378. Available online: www.proceedings.com (accessed on 15 July 2021).
22. Torres, E.M.G.; Águila, A.; Isaac, I.; González, J.W.; López, G. Analysis of Voltage Profile to determine Energy Demand using Monte Carlo algorithms and Markov Chains (MCMC). In Proceedings of the 51st International Universities Power Engineering Conference (UPEC), Coimbra, Portugal, 6–9 September 2016; pp. 1–6. [[CrossRef](#)]
23. Nusair, K.; Alasali, F.; Hayajneh, A.; Holderbaum, W. Optimal placement of FACTS devices and power-flow solutions for a power network system integrated with stochastic renewable energy resources using new metaheuristic optimization techniques. *Int. J. Energy Res.* **2021**, *45*, 18786–18809. [[CrossRef](#)]
24. Singh, B.; Agrawal, G. Enhancement of voltage profile by incorporation of SVC in power system networks by using optimal load flow method in MATLAB/Simulink environments. *Energy Rep.* **2018**, *4*, 418–434. [[CrossRef](#)]
25. Kamel, S.; Youssef, H. Voltage Stability Enhancement Based on Optimal Allocation of Shunt Compensation Devices Using Lightning Attachment Procedure Optimization. *Int. J. Interact. Multimed. Artif. Intell.* **2019**, *5*, 125. [[CrossRef](#)]
26. Bhayani, K.J.; Pandya, D.J. Optimal Allocation of FACTS Devices Using Kinetic Gas Molecular Optimization and Cuckoo Search Algorithm. *J. Inst. Eng. (India) Ser. B* **2022**, *103*, 2057–2072. [[CrossRef](#)]
27. Yasin, N.M.; Talib, H.A. Genetic Based Optimal Location of STATCOM Compensator. *Int. J. Appl. Eng. Res.* **2018**, *13*, 7516–7521.
28. Salama, H.S.; Vokony, I. Voltage stability indices—A comparison and a review. *Comput. Electr. Eng.* **2022**, *98*, 107743. [[CrossRef](#)]

29. Zaheb, H.; Danish, M.S.S.; Senjyu, T.; Ahmadi, M.; Nazari, A.M.; Wali, M.; Khosravy, M.; Mandal, P. A contemporary novel classification of voltage stability indices. *Appl. Sci.* **2020**, *10*, 1639. [[CrossRef](#)]
30. Nadeem, M.; Imran, K.; Khattak, A.; Ulasyar, A.; Pal, A.; Zeb, M.Z.; Khan, A.N.; Padhee, M. Optimal placement, sizing and coordination of FACTS devices in transmission network using whale optimization algorithm. *Energies* **2020**, *13*, 753. [[CrossRef](#)]
31. Hemeida, M.G.; Rezk, H.; Hamada, M.M. A comprehensive comparison of STATCOM versus SVC-based fuzzy controller for stability improvement of wind farm connected to multi-machine power system. *Electr. Eng.* **2018**, *100*, 935–951. [[CrossRef](#)]
32. Modarresi, J.; Gholipour, E.; Khodabakhshian, A. A comprehensive review of the voltage stability indices. *Renew. Sustain. Energy Rev.* **2016**, *63*, 1–12. [[CrossRef](#)]
33. Danish, M.S.S.; Senjyu, T.; Danish, S.M.S.; Sabory, N.R.; Narayanan, K.; Mandal, P. A recap of voltage stability indices in the past three decades. *Energies* **2019**, *12*, 1544. [[CrossRef](#)]
34. Shojaei, A.H.; Ghadimi, A.A.; Miveh, M.R.; Mohammadi, F.; Jurado, F. Multi-Objective Optimal Reactive Power Planning under Load Demand and Wind Power Generation Uncertainties Using ϵ -Constraint Method. *Appl. Sci.* **2020**, *10*, 2859. [[CrossRef](#)]
35. Daqaq, F.; Ouassaid, M.; Ellaia, R. A new meta-heuristic programming for multi-objective optimal power flow. *Electr. Eng.* **2021**, *103*, 1217–1237. [[CrossRef](#)]
36. Conejo, A.J.; Baringo, L. *Power System Operations*; Springer International Publishing: Cham, Switzerland, 2018. [[CrossRef](#)]
37. Pandian, A.N.; Palanivelu, A. Metaheuristic optimization based placement of SVCs with multiple objectives. *J. Eng. Des. Technol.* **2021**, *19*, 1586–1600. [[CrossRef](#)]
38. Čalasan, M.; Konjić, T.; Kecojević, K.; Nikitović, L. Optimal allocation of static var compensators in electric power systems. *Energies* **2020**, *13*, 3219. [[CrossRef](#)]
39. Vanishree, J.; Ramesh, V. Optimization of size and cost of Static VAR Compensator using Dragonfly algorithm for voltage profile improvement in power transmission systems. *Int. J. Renew. Energy Res.* **2018**, *8*, 56–66. [[CrossRef](#)]
40. Villa-Acevedo, W.M.; LópezLezama, J.M.; Colomé, D.G.; Cepeda, J. Long-term voltage stability monitoring of power system areas using a kernel extreme learning machine approach. *Alex. Eng. J.* **2022**, *61*, 1353–1367. [[CrossRef](#)]
41. Wolgast, T.; Ferenz, S.; Nieße, A. Reactive Power Markets: A Review. *IEEE Access* **2022**, *10*, 28397–28410. [[CrossRef](#)]
42. Guascal, A. Mejora del margen de estabilidad de tensión en sistemas de potencia basado en la ubicación óptima de dispositivos SVC. Bachelor's Thesis, Universidad Politécnica Salesiana, Cuenca, Ecuador, 2020.
43. Vaca, S.; Gallardo, C. Secondary Voltage Control Areas Using Hybrid Methods for Systems with High Wind Penetration. In *Latest Advances in Electrical Engineering, and, Electronics*; Botto-Tobar, M., Vizuete, M.Z., Cadena, A.D., Vizuete, A.Z., Eds.; Springer International Publishing: Cham, Switzerland, 2022; Volume 933, pp. 17–32. [[CrossRef](#)]
44. Alayande, A.S.; Nwulu, N. A novel approach for the identification of critical nodes and transmission lines for mitigating voltage instability in power networks. *Afr. J. Sci. Technol. Innov. Dev.* **2019**, *11*, 383–390. [[CrossRef](#)]
45. Alzaareer, K.; Saad, M.; Mehrjerdi, H.; Lefebvre, S.; Asber, D. TopDown/Bottom-Up Method for Identifying a Set of Voltage Stability Preventive Controls. In Proceedings of the 2020 International Conference on Technology and Policy in Energy and Electric Power (ICT-PEP), Bandung, Indonesia, 23–24 September 2020; Volume 3, pp. 339–343. [[CrossRef](#)]
46. Chakraborty, K.; Chakrabarti, A. *Chakrabarti, Soft Computing Techniques in Voltage Security Analysis*; Springer: New Delhi, India, 2015. [[CrossRef](#)]

Disclaimer/Publisher's Note: The statements, opinions and data contained in all publications are solely those of the individual author(s) and contributor(s) and not of MDPI and/or the editor(s). MDPI and/or the editor(s) disclaim responsibility for any injury to people or property resulting from any ideas, methods, instructions or products referred to in the content.